

On the Effectiveness of Low Frequency Perturbations

Yash Sharma, Gavin Weiguang Ding, and Marcus A. Brubaker

Borealis AI

Abstract

Carefully crafted, often imperceptible, adversarial perturbations have been shown to cause state-of-the-art models to yield extremely inaccurate outputs, rendering them unsuitable for safety-critical application domains. In addition, recent work has shown that constraining the attack space to a low frequency regime is particularly effective. Yet, it remains unclear whether this is due to generally constraining the attack search space or specifically removing high frequency components from consideration. By systematically controlling the frequency components of the perturbation, evaluating against the top-placing defense submissions in the NeurIPS 2017 competition, we empirically show that performance improvements in both optimization and generalization are yielded only when low frequency components are preserved. In fact, the defended models based on (ensemble) adversarial training are roughly as vulnerable to low frequency perturbations as undefended models, suggesting that the purported robustness of proposed defenses is reliant upon adversarial perturbations being high frequency in nature. We do find that under $\ell_\infty \epsilon = 16/255$, a commonly used distortion bound, low frequency perturbations are indeed perceptible. This questions the use of the ℓ_∞ -norm, in particular, as a distortion metric, and suggests that explicitly considering the frequency space is promising for learning robust models which better align with human perception.

1 Introduction

Despite the impressive performance deep neural networks have shown, researchers have discovered that they are, in some sense, ‘brittle’; small carefully crafted ‘adversarial’ perturbations to their inputs can result in wildly different outputs (Szegedy et al., 2013; Biggio et al., 2013). Even worse, these perturbations have been shown to *transfer*: learned models can be successfully manipulated by adversarial perturbations generated by attacking distinct models. An attacker can discover a model’s vulnerabilities even without access to it.

The goal of this paper is to investigate the relationship between a perturbation’s frequency properties and its effectiveness, and is motivated by recent work showing the effectiveness of low frequency perturbations in particular. Guo et al. (2018) shows that constraining the perturbation to the low frequency subspace improves the query efficiency of the decision-based gradient-free boundary attack (Brendel et al., 2017). Zhou et al. (2018) achieves improved transferability by suppressing high frequency components of the perturbation. Similarly, the winning entry of the CAAD 2018 competition¹ applies a 2D Gaussian filter on the gradient w.r.t. the input image during the iterative optimization process (Sharma et al., 2018). This ‘spatial smoothing’ operation acts as a ‘low-pass filter’ in the frequency domain of the perturbation.

However, two questions still remain unanswered:

¹Competition on Adversarial Attacks and Defenses: <http://hof.geekpwn.org/caad/en/index.html>.

1. whether the effectiveness of low frequency perturbations is due to *the reduced search space* or *the low frequency components*? and
2. under what conditions are low frequency perturbations more effective than unconstrained perturbations?

To answer these questions, we design systematic experiments to test the effectiveness of perturbations manipulating specified frequency components, utilizing the discrete cosine transform (DCT). Testing against state-of-the-art defense methods, we show that, when perturbations are constrained to the low frequency subspace, they are 1) generated faster; and 2) more transferable. However, if perturbations are constrained to other frequency subspaces, they perform worse in general, which confirms the effectiveness of low frequency perturbations is due to specifically focusing on low frequency components rather than reducing the dimensionality of the search space in general. On the other hand, we also notice that the improved effectiveness of low frequency perturbations is only significant for defended models, but not for clean models. Finally, based on the perceptual difference between the unconstrained and low frequency attacks, we discuss the problem of using the commonly used ℓ_∞ norm as a perceptual metric for quantifying robustness, and also the possibilities of utilizing frequency properties to learn robust models which better align with human perception.

2 Background

Generating adversarial examples is an optimization problem, while generating transferable adversarial examples is a generalization problem. The optimization variable is the perturbation, and the objective is to fool the model, while constraining (or minimizing) the magnitude of the perturbation. ℓ_p norms are typically used to quantify the strength of the perturbation; though they are well known to be poor perceptual metrics (Zhang et al., 2018), constraint magnitudes used in practice are assumed to be small enough such that the ball is a subset of the imperceptible region.

Adversarial perturbations can be crafted in not only the white-box setting (Carlini & Wagner, 2017b; Chen et al., 2017a) but in limited access settings as well (Chen et al., 2017b; Alzantot et al., 2018a). When querying the model is not possible, attacks must rely on transferability. Finally, adversarial perturbations are not a continuous phenomenon, recent work has shown applications in discrete settings (e.g. natural language) (Alzantot et al., 2018b; Lei et al., 2018).

Numerous defenses have been proposed, to limited success. Many have been found to be easily circumvented (Carlini & Wagner, 2017a; Sharma & Chen, 2018; Athalye et al., 2018), while others have been unable to scale to high-dimensional complex datasets, e.g. ImageNet (Smith & Gal, 2018; Papernot & McDaniel, 2018; Li et al., 2018; Schott et al., 2018). Adversarial training, training the model with adversarial examples (Goodfellow et al., 2014; Tramèr et al., 2017; Madry et al., 2017; Ding et al., 2018), has demonstrated improvement, but is limited to the properties of the perturbations used, e.g. training exclusively on ℓ_∞ does not provide robustness to perturbations generated under other distortion metrics (Sharma & Chen, 2017). In both the NeurIPS 2017 and CAAD 2018 competitions, which used ImageNet, winning defenses built upon these trained models to reduce their vulnerabilities (Kurakin et al., 2018; Sharma et al., 2018; Xie et al., 2018).

3 Methods

Here, we describe the attack we experiment with and how to constrain the perturbation to specified frequency subspaces.

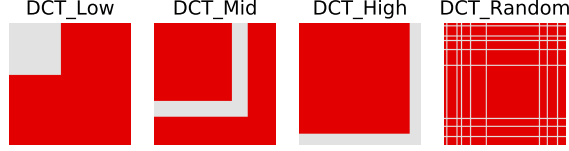


Figure 1: Masks used to constrain the frequency space where $n = 128$ and $d = 299$ (ImageNet). Red denotes frequency components of the perturbation which will be masked when generating the adversarial example, both during and after the optimization process.

| | |
|-------|---|
| Cln_1 | [InceptionV3] |
| Cln_3 | [InceptionV3, InceptionV4, ResNetV2_101] |
| Adv_1 | [AdvInceptionV3] |
| Adv_3 | [AdvInceptionV3, Ens3AdvInceptionV3, Ens4AdvInceptionV4] |

Table 1: Models used for generating black-box attacks.

3.1 Attacks

We consider ℓ_∞ -norm constrained perturbations, where the perturbation δ satisfies $\|\delta\|_\infty \leq \epsilon$, with ϵ being the maximum perturbation magnitude. Specifically, we choose to use the Momentum Iterative Method (MIM) (Dong et al., 2017), which has been shown to be the best performing attack in the previously mentioned NeurIPS 2017 and CAAD 2018 competitions. MIM is an iterative attack where each step of it involves the Fast Gradient Sign Method (FGSM) (Goodfellow et al., 2014). The FGSM perturbation is a simple, one-step gradient-based perturbation generated as:

$$\delta_{\text{FGSM}} = s \cdot \epsilon \cdot \text{sign}(\nabla_x J(x, y)) \quad (1)$$

where x is the input image, J is the classification loss function, $\text{sign}(\cdot)$ is the element-wise sign function². When y is the true label of x and $s = +1$, δ is the *non-targeted* attack for misclassification; when y is a *target* label other than the true label of x and $s = -1$, δ is the *targeted* attack for manipulating the network to wrongly predict y . Briefly speaking, MIM improves FGSM in two aspects: 1) it runs for multiple iterations which helps in maximizing a non-linear loss function; 2) it replaces the gradient $\nabla_x J(x, y)$ with a “momentum” term to prevent the “overfitting” problem, caused by poor local optima, in order to improve transferability.

3.2 Frequency Constraints

Our goal is to examine whether the effectiveness of low frequency perturbations is due to a reduced search space in general or specifically due to focusing on low frequency components. To achieve this, we use the *discrete cosine transform* (DCT) (Rao & Yip, 2014) to constrain the perturbation to only modify certain frequency components of the input. The DCT decomposes a signal into cosine wave components with different frequencies and amplitudes. Given a 2D image (or perturbation) $x \in \mathbb{R}^{d \times d}$, the DCT Transform of x is $v = \text{DCT}(x)$, where the entry $v_{i,j}$ is the magnitude of its corresponding basis functions. The numerical values of i and j represent the frequencies, i.e. smaller values represent lower frequencies and vice versa. The DCT is invertible, with an inverse transform $x = \text{IDCT}(v)$ ³.

²sign = 1 if $x > 0$, sign = -1 if $x < 0$, sign = 0, if $x = 0$.

³DCT / IDCT is applied to each color channel independently.

We remove certain frequency components of the perturbation δ by applying a mask to its DCT transform $\text{DCT}(\delta)$. We then reconstruct the perturbation by applying IDCT on the masked DCT transform. Specifically, the mask, $m \in \{0, 1\}^{d \times d}$, is a 2D matrix image whose pixel values are 0’s and 1’s, and the “masking” is done by element-wise product. We can then reconstruct the “transformed” perturbation by applying the IDCT to the masked DCT(δ). The entire transformation can then be represented as:

$$\text{FreqMask}(\delta) = \text{IDCT}(\text{Mask}(\text{DCT}(\delta))) . \quad (2)$$

Accordingly in MIM, we use the following gradient

$$\nabla_{\delta} J(x + \text{FreqMask}(\delta), y) .$$

We use 4 different FreqMask types to constrain the perturbations, as shown in Figure 1. `DCT_High` only preserves high frequency components; `DCT_Low` only preserves low frequency components; `DCT_Mid` only preserves mid frequency components; and `DCT_Rand` preserves randomly sampled components. For reduced dimensionality n , we preserve $n \times n$ components. Recall that $v = \text{DCT}(x)$, `DCT_Low` preserves components $v_{i,j}$ if $1 \leq i, j \leq n$; `DCT_High` masks components if $1 \leq i, j \leq \sqrt{d^2 - n^2}$; `DCT_Mid` and `DCT_Rand` also preserve $n \times n$ components, the detailed generation processes can be found in the appendix. Figure 1 visualizes the masks when $d = 299$ (e.g. ImageNet) and $n = 128$. Note that when $n = 128$, we only preserve $128^2/299^2 \approx 18.3\%$ of the frequency components, a small fraction of the original unconstrained perturbation.

4 Results and Analyses

To evaluate the effectiveness of perturbations under frequency constraints, we test against top defenses from the NeurIPS 2017 Adversarial Attacks and Defences Competition (Kurakin et al., 2018).

Threat Models: We evaluate attacks in both the non-targeted and targeted case, and measure the attack success rate (ASR) on 1000 test examples. We test on $\epsilon = 16/255$ and iterations = $[1, 10]$ for the non-targeted case, and $\epsilon = 32/255$ and iterations = 10 for the targeted case. $\epsilon = 16/255$ and $\epsilon = 32/255$ were the maximum distortions allowed in the NeurIPS 2017 and CAAD 2018 competitions, respectively. The magnitude for the targeted case is larger since targeted attacks, particularly on ImageNet (1000 classes), are significantly harder.

Attacks: As described in Section 3, we experiment with the original unconstrained MIM and frequency constrained MIM with masks shown in Figure 1. For each mask type, we test $n = [256, 128, 64, 32]$ with $d = 299$. For `DCT_Rand`, we average results over 3 random seeds.

To describe the attack settings, we specify model placeholders A and B . We call an attack *white-box*, when we attack model A with the perturbation generated from A itself. We call an attack *grey-box*, when the perturbation is generated from A , but used to attack a “defended” A , where a defense module is prepended to A . We call an attack *black-box*, when the perturbation generated from A is used to attack distinct B , where B can be defended or not.

Target Models and Defenses for Evaluation: We evaluate each of the attack settings against models and defenses chosen from the top defense solutions in the NeurIPS 2017 competition (Kurakin et al., 2018). Each of the top-4 NeurIPS 2017 defenses prepend a tuned (or trained) preprocessor to an ensemble of classifiers, which for all of them included the strongest available adversarially trained model:

EnsAdvInceptionResNetV2⁴ (Tramèr et al., 2017). Thus, we use EnsAdvInceptionResNetV2 to benchmark the robustness⁵ of adversarially trained models.

We then prepend the preprocessors from the top-4 NeurIPS 2017 defenses to EnsAdvInceptionResNetV2, and denote the defended models as D1, D2, D3, and D4, respectively. Regarding the preprocessors, D1 uses a trained denoiser where the loss function is defined as the difference between the target model’s outputs activated by the clean image and denoised image (Liao et al., 2017); D2 uses random resizing and random padding (Xie et al., 2017); D3 uses a number of image transformations: shear, shift, zoom, and rotation (Thomas & Elibol, 2017); and D4 simply used median smoothing (Kurakin et al., 2018).

For our representative cleanly trained model, we evaluate against the state-of-the-art NasNetLarge_331⁶ (Zoph et al., 2017). We denote EnsAdvInceptionResNetV2⁵ as EnvAdv and NasNetLarge_331⁷ as NasNet for brevity.

Source Models for Perturbation Generation: For white-box attacks, we use perturbations generated from NasNet and EnsAdv to attack themselves respectively. For grey-box attacks, we use perturbations generated from EnsAdv to attack D1, D2, D3, and D4 respectively. For black-box attacks, since the models for generating the perturbations need to be distinct from the ones being attacked, we use 4 different sources (ensembles) which vary in ensemble size and whether the models are adversarially trained or cleanly trained, as shown in Table 1. In summary, for black-box attacks, perturbations generated from Adv_1, Adv_3, Cln_1, and Cln_3 are used to attack NasNet, EnsAdv, D1, D2, D3, and D4.

4.1 Overview of the Results

As described, we test the unconstrained and constrained perturbations in the white-box, grey-box, and black-box scenarios. Representative results are shown in Figure 2a, 2b, 2c, and 2d. In each of these plots, the vertical axis is attack success rate (ASR), while the horizontal indicates the number of frequency components kept (Dimensionality). Unconstrained MIM is shown as a horizontal line across the dimensionality axis for ease of comparison. In each figure, the plots are, from left to right, non-targeted attack with iterations = 1, non-targeted with iterations = 10, and targeted with iterations = 10. From these figures, we can see that DCT_Low always outperforms the other frequency constraints, including DCT_High, DCT_Mid and DCT_Rand. This confirms that the effectiveness of low frequency perturbations is not due to a general restriction of search space, but due to the low frequency regime itself. Thus, in our remaining experiments, we focus on low frequency constrained perturbations, i.e. DCT_Low.

We compare ASR and relative changes across all black-box transfer pairs between standard unconstrained MIM and MIM constrained with DCT_Low $n = 128$, on non-targeted attacks with both iterations = 1 and iterations = 10. This comparison is visualized in Figure 3 and 4.

4.2 Observations and Analyses

DCT_Low generates effective perturbations faster on adversarially trained models, but not on cleanly trained models. Figure 2a and 2b show the white-box ASRs on EnsAdv and NasNet respectively. For EnsAdv, we can see that DCT_Low improves ASR in the non-targeted case with iterations = 1 and in the targeted case with iterations = 10, but not in the non-targeted case with iterations = 10. However, in this case, DCT_Low still outperforms other frequency constraints and does not significantly deviate from unconstrained MIM’s performance. When the number of iterations is large enough that unconstrained MIM can succeed consistently, constraining the space only limits the attack, but otherwise, the low frequency

⁴https://github.com/tensorflow/models/tree/master/research/adv_imagenet_models

⁵EnsAdvInceptionResNetV2 is to be attacked.

⁶<https://github.com/tensorflow/models/tree/master/research/slim>

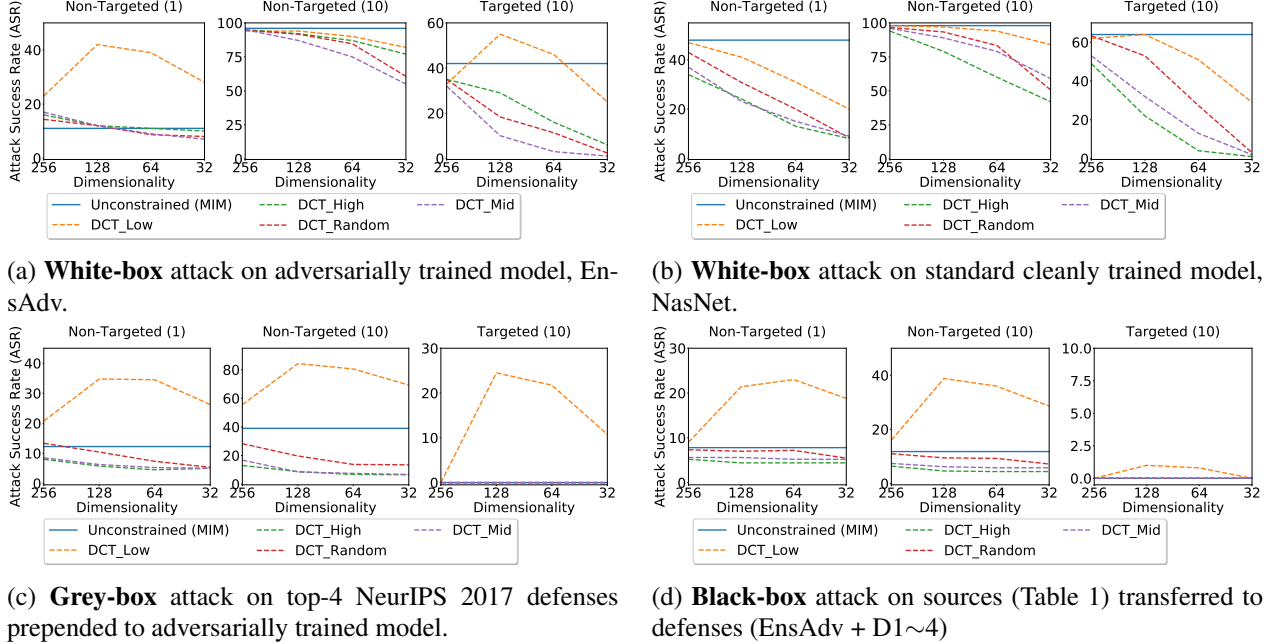


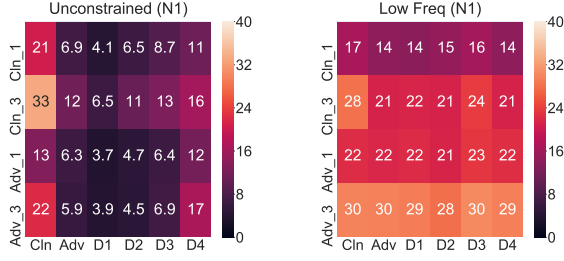
Figure 2: Number of iterations in parentheses. Non-targeted with $\epsilon = 16/255$, targeted with $\epsilon = 32/255$.

prior is effective. Therefore, low frequency perturbations are more “iteration efficient”, as they can be found more easily with a less exhaustive search, which is practically helpful computationally.

However, for white-box attacks on NasNet in Figure 2b, we see that although `DCT_Low` still outperforms the other frequency constraints, it does perform worse than unconstrained MIM. Comparing Figure 2a and 2b, it is clear that `DCT_Low` performs similarly against the adversarially trained model and the cleanly trained model, the difference here is due to unconstrained MIM performing significantly better against the cleanly trained model than against the adversarially trained model. This implies that the low frequency prior is useful against defended models, in particular, since it exploits the space where adversarial training, which is necessarily imperfect, fails to reduce vulnerabilities.

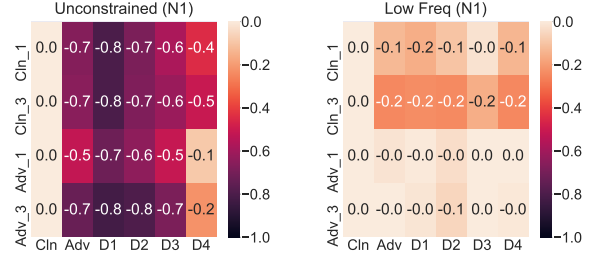
DCT_Low bypasses defenses prepended to the adversarially trained model. As previously mentioned, in the grey-box case, we generate the perturbations from the undefended EnsAdv and use them to attack D1, D2, D3 and D4 (which include preprocessors prepended to EnsAdv). Figure 2c shows the ASR results averaged over D1~4. `DCT_Low` outperforms unconstrained MIM by large margins in all cases. Comparing Figure 2a with Figure 2c, the larger difference between unconstrained MIM and `DCT_Low` in the grey-box case reflects the fact that the top NeurIPS 2017 defenses are not nearly as effective against low frequency perturbations as they are against standard unconstrained attacks. In fact, `DCT_Low` yields the same ASR on D1, the winning defense submission in the NeurIPS 2017 competition, as on the adversarially trained model without the preprocessor prepended; the preprocessors are not effective (at all) at protecting the model from low frequency perturbations, even in the targeted case, where success is only yielded if the model is fooled to predict, out of all 1000 class labels, the specified target label. Results against the individual defenses are in the appendix.

DCT_Low helps black-box transfer to defended models. For assessing black-box transferability, we use Cln_1, Cln_3, Adv_1, Adv_3 in Table 1 as the source models for generating perturbations, and attack EnsAdv and D1~4, resulting in 20 source-target pairs in total. The average ASR results over these pairs are reported



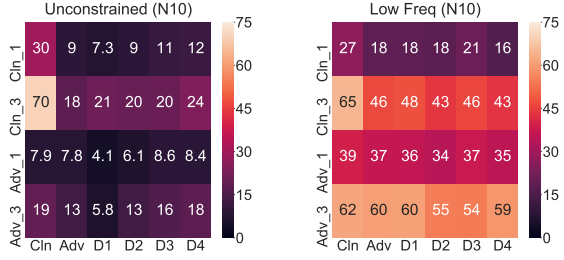
(a)

(b)



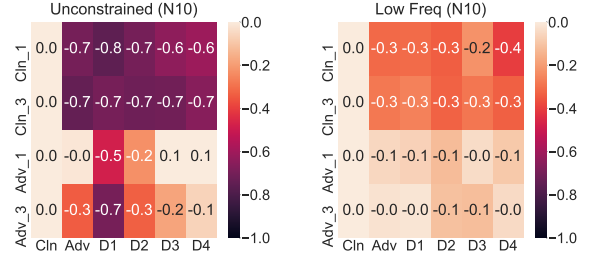
(a)

(b)



(c)

(d)



(c)

(d)

Figure 3: Transferability matrices with attack success rates (ASRs), comparing unconstrained MIM with low frequency constrained DCT_{Low} ($n = 128$) in the non-targeted case. First row is with iterations = 1, second is with iterations = 10. The column Cln is NasNet, Adv is EnsAdv.

Figure 4: Transferability matrices with attack relative difference in ASR with the Cln model (first column). Rows and columns in each subfigure is indexed in the same way as Figure 3.

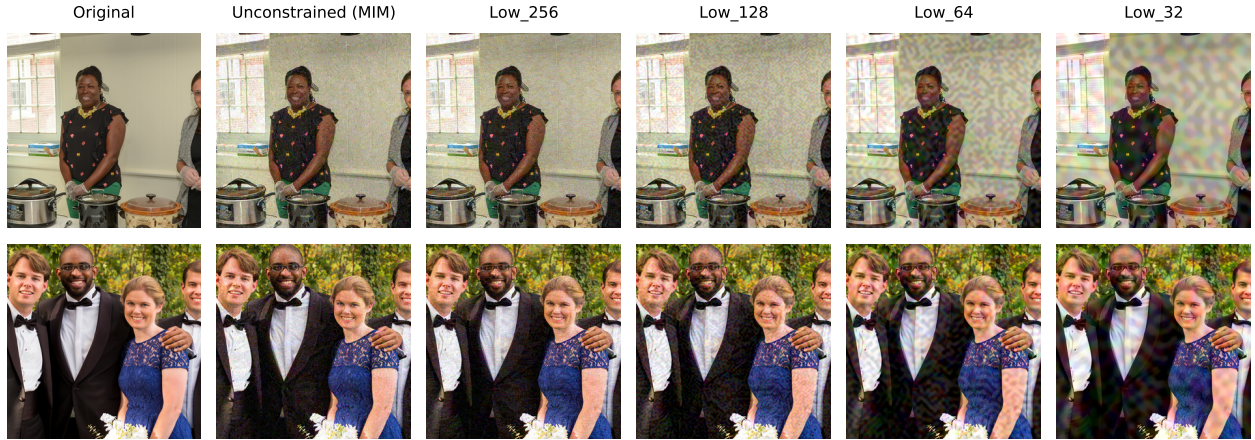


Figure 5: Adversarial examples generated with $\ell_\infty \epsilon = 16/255$ distortion

in Figure 2d. In the non-targeted case, we again see that DCT_{Low} significantly outperforms unconstrained MIM. However, in the targeted case, constraining to the low frequency subspace does not enable MIM to

succeed in transferring to distinct black-box defended models due to the difficult nature of targeted transfer⁷.

Next, we look at individual source-target pairs. For each pair, we compare `DCT_Low` ($n = 128$) with unconstrained MIM in the non-targeted case with iterations = 1 and iterations = 10. Results for all frequency configurations are provided in the appendix. Figure 3 shows the transferability matrices for all source-target pairs, where for each subplot, the row indices denote source models, and the column indices denote target models. The value (and associated color) in each gridcell represent the ASR for the specified source-target pair. For Figure 4, the gridcell values represent the relative difference in ASR between the target model and the cleanly trained model (`Cln`)⁸, using the source model of the corresponding row.

Comparing (a) to (b) and (c) to (d) in Figure 3, it is clear that low frequency perturbations are much more effective than unconstrained MIM against defended models. Specifically, we can see that `DCT_Low` is significantly more effective than unconstrained MIM against `EnsAdv`, and `D1~4` provide almost no additional robustness to `EnsAdv` when low frequency perturbations are applied.

`DCT_Low` is not effective when transferring between undefended cleanly trained models. However, we do observe that `DCT_Low` does not improve black-box transfer between undefended cleanly trained models, which can be seen by comparing indices (`Cln_1,Cln`) and (`Cln_3,Cln`) between Figure 3 (a) and (b), as well as (c) and (d). As discussed when comparing white-box performance against cleanly trained and adversarially trained models, low frequency constraints are not generally more effective, but instead exploit the vulnerabilities in currently proposed defenses.

4.3 Effectiveness of Low Frequency on Undefended v.s. Defended Models

In the last section, we showed that `DCT_Low` is highly effective against adversarially trained models and top-performing preprocessor-based defenses, in white-box, grey-box and black-box cases. However, low frequency does not help when only cleanly trained models are involved, i.e. white-box on clean models and black-box transfer between clean models. To explain this phenomenon, we hypothesize that the considered state-of-the-art ImageNet defenses do not reduce vulnerabilities within the low frequency subspace, and thus `DCT_Low` is roughly as effective against defended models as against clean models, a property not seen when evaluating with standard, unconstrained attacks.

This can be most clearly seen in Figure 4, which presents the normalized difference between ASR on each of the target models with ASR on the cleanly trained model. The difference is consistently smaller for `DCT_Low` than for unconstrained MIM, and nearly nonexistent when the perturbations were generated against adversarially trained (defended) models (`Adv_1,Adv_3`). Thus, as discussed, defended models are roughly as vulnerable as undefended models when encountered by low frequency perturbations.

5 Discussion

Our experiments show that the results seen in recent work on the effectiveness of constraining the attack space to low frequency components (Guo et al., 2018; Zhou et al., 2018; Sharma et al., 2018) are not due to generally reducing the size of the attack search space. When evaluating against state-of-the-art adversarially trained models and winning defense submissions in the NeurIPS 2017 competition in the white-box, grey-box, and black-box settings, significant improvements are only yielded when low frequency components of

⁷Note that though the NeurIPS 2017 and CAAD 2018 competitions were proposed in the black-box setting, where submitted attacks are evaluated against unknown submitted defenses, in practice the attackers were able to predict classifiers used by defenders, due to the computational difficulty in training ImageNet models. This transforms the attack setting to the grey-box case, where we have seen low frequency perturbations are able to succeed at a high rate, explaining the winning submission in the CAAD 2018 competition being an application of spatial smoothing (Sharma et al., 2018).

⁸The relative difference for the target model = (ASR on the target model - ASR on `Cln`) / ASR on `Cln`.

the perturbation are preserved. Low frequency perturbations are so effective that they render state-of-the-art ImageNet defenses to be roughly as vulnerable as undefended, cleanly trained models under attack.

However, we also noticed that low frequency perturbations do not improve performance when defended models are not involved, seen in evaluating white-box performance against and black-box transfer between cleanly trained models. Low frequency perturbations do not yield faster white-box attacks on clean models, nor do they provide more effective transfer between clean models.

Our results suggest that the state-of-the-art ImageNet defenses, based on necessarily imperfect adversarial training, only significantly reduce vulnerability outside of the low frequency subspace, but not so much within. Against defenses, low frequency perturbations are more effective than unconstrained ones since they exploit the vulnerabilities which purportedly robust models share. Against undefended models, constraining to a subspace of significantly reduced dimensionality is unhelpful, since undefended models share vulnerabilities beyond the low frequency subspace. Understanding whether this observed vulnerability in defenses is caused by an intrinsic difficulty to being robust in the low frequency subspace, or simply due to the (adversarial) training procedure rarely sampling from the low frequency region is an interesting direction for further work.

Low frequency perturbations are perceptible (under ℓ_∞ -norm $\epsilon = 16/255$). Our results show that the robustness of currently proposed ImageNet defenses relies on the assumption that adversarial perturbations are high frequency in nature. Though the adversarial defense problem is not constrained to achieving robustness to imperceptible perturbations, this is a reasonable first step. Thus, in Figure 5, we visualize low frequency constrained adversarial examples under commonly used ℓ_∞ -norm constraint $\epsilon = 16/255$. Though the perturbations do not significantly change human perceptual judgement, e.g. the top example still appears to be a standing woman, the perturbations with $n \leq 128$ are indeed perceptible.

Although it is well-known that ℓ_p -norms (in input space) are far from metrics aligned with human perception, exemplified by their widespread use, it is still assumed that with a small enough bound (e.g. $\ell_\infty \epsilon = 16/255$), the resulting ball will constitute a subset of the imperceptible region. The fact that low frequency perturbations are fairly visible challenges this common belief. In addition, if the goal is robustness to imperceptible perturbations, our study suggests this might be achieved, without adversarial training, by relying on low frequency components, yielding a much more computationally practical training procedure. In all, we hope our study encourages researchers to not only consider the frequency space, but perceptual priors in general, when bounding perturbations and proposing tractable, reliable defenses.

References

- M. Alzantot, Y. Sharma, S. Chakraborty, and M. Srivastava. Genattack: Practical black-box attacks with gradient-free optimization. *arXiv preprint arXiv:1805.11090*, 2018a.
- M. Alzantot, Y. Sharma, A. Elgohary, B. Ho, M. Srivastava, and K. Chang. Generating natural language adversarial examples. *arXiv preprint arXiv:1804.07998*, 2018b.
- A. Athalye, N. Carlini, and D. Wagner. Obfuscated gradients give a false sense of security: Circumventing defenses to adversarial examples. *arXiv preprint arXiv:1802.00420*, 2018.
- B. Biggio, I. Corona, D. Maiorca, B. Nelson, N. Šrđić, P. Laskov, G. Giacinto, and F. Roli. Evasion attacks against machine learning at test time. In *ECML PKDD*, pp. 387–402. Springer, 2013.
- W. Brendel, J. Rauber, and M. Bethge. Decision-based adversarial attacks: Reliable attacks against black-box machine learning models. *arXiv preprint arXiv:1712.04248*, 2017.

- N. Carlini and D. Wagner. Adversarial examples are not easily detected: Bypassing ten detection methods. *arXiv preprint arXiv:1705.07263*, 2017a.
- N. Carlini and D. Wagner. Towards evaluating the robustness of neural networks. *arXiv preprint arXiv:1608.04644*, 2017b.
- P. Y. Chen, Y. Sharma, H. Zhang, J. Yi, and C. Hsieh. Ead: Elastic-net attacks to deep neural networks via adversarial examples. *arXiv preprint arXiv:1709.0414*, 2017a.
- P. Y. Chen, H. Zhang, Y. Sharma, J. Yi, and C. Hsieh. Zoo: Zeroth order optimization based black-box attacks to deep neural networks without training substitute models. In *AISeC '17*, pp. 15–26. ACM, 2017b.
- G. W. Ding, Y. Sharma, K. Lui, and R. Huang. Max-margin adversarial (mma) training: Direct input space margin maximization through adversarial training. *arXiv preprint arXiv:1812.02637*, 2018.
- Y. Dong, F. Liao, T. Pang, H. Su, J. Zhu, X. Hu, and J. Li. Boosting adversarial attacks with momentum. *arXiv preprint arXiv:1710.06081*, 2017.
- I. Goodfellow, J. Shlens, and C. Szegedy. Explaining and harnessing adversarial examples. *arXiv preprint arXiv:1412.6572*, 2014.
- C. Guo, J. Frank, and K. Weinberger. Low frequency adversarial perturbation. *arXiv preprint arXiv:1809.08758*, 2018.
- A. Kurakin, I. Goodfellow, S. Bengio, et al. Adversarial attacks and defences competition. *arXiv preprint arXiv:1804.00097*, 2018.
- Q. Lei, L. Wu, P. Y. Chen, A. Dimakis, I. Dhillon, and M. Witbrock. Discrete attacks and submodular optimization with applications to text classification. *arXiv preprint arXiv:1812.00151*, 2018.
- Y. Li, J. Bradshaw, and Y. Sharma. Are generative classifiers more robust to adversarial attacks? *arXiv preprint arXiv:1802.06552*, 2018.
- F. Liao, M. Liang, Y. Dong, T. Pang, X. Hu, and J. Zhu. Defense against adversarial attacks using high-level representation guided denoiser. *arXiv preprint arXiv:1712.02976*, 2017.
- A. Madry, A. Makelov, L. Schmidt, D. Tsipras, and A. Vladu. Towards deep learning models resistant to adversarial attacks. *arXiv preprint arXiv:1706.06083*, 2017.
- N. Papernot and P. McDaniel. Deep k-nearest neighbors: Towards confident, interpretable and robust deep learning. *arXiv preprint arXiv:1803.04765*, 2018.
- K Ramamohan Rao and Ping Yip. *Discrete cosine transform: algorithms, advantages, applications*. Academic press, 2014.
- L. Schott, J. Rauber, M. Bethge, and W. Brendel. Towards the first adversarially robust neural network model on mnist. *arXiv preprint arXiv:1805.09190*, 2018.
- Y. Sharma and P. Y. Chen. Attacking the madry defense model with l1-based adversarial examples. *arXiv preprint arXiv:1710.10733*, 2017.
- Y. Sharma and P. Y. Chen. Bypassing feature squeezing by increasing adversary strength. *arXiv preprint arXiv:1803.09868*, 2018.

- Y. Sharma, T. Le, and M. Alzantot. Caad 2018: Generating transferable adversarial examples. *arXiv preprint arXiv:1810.01268*, 2018.
- L. Smith and Y. Gal. Understanding measures of uncertainty for adversarial example detection. *arXiv preprint arXiv:1803.08533*, 2018.
- C. Szegedy, W. Zaremba, I. Sutskever, J. Bruna, D. Erhan, and I. Goodfellow. Intriguing properties of neural networks. *arXiv preprint arXiv:1312.6199*, 2013.
- A. Thomas and O. Elibol. Defense against adversarial attack: 3rd place. <https://github.com/anlthms/nips-2017>, 2017.
- F. Tramèr, A. Kurakin, N. Papernot, D. Boneh, and P. McDaniel. Ensemble adversarial training: Attacks and defenses. *arXiv preprint arXiv:1705.07204*, 2017.
- C. Xie, J. Wang, Z. Zhang, Z. Ren, and A. Yuille. Mitigating adversarial effects through randomization. *arXiv preprint arXiv:1711.01991*, 2017.
- C. Xie, Y. Wu, L. van der Maaten, A. Yuille, and K. He. Feature denoising for improving adversarial robustness. *arXiv preprint arXiv:1812.03411*, 2018.
- R. Zhang, P. Isola, A. Efros, E. Shechtman, and O. Wang. The unreasonable effectiveness of deep features as a perceptual metric. *arXiv preprint arXiv:1801.03924*, 2018.
- W. Zhou, X. Hou, Y. Chen, M. Tang, X. Huang, X. Gan, and Y. Yang. Transferable adversarial perturbations. In *ECCV (14)*, pp. 471–486. Springer, 2018.
- B. Zoph, V. Vasudevan, J. Shlens, and Q. Le. Learning transferable architectures for scalable image recognition. *arXiv preprint arXiv:1707.07012*, 2017.

6 Appendix

6.1 Construction Process

For a specified reduced dimensionality n , and original dimensionality d , we consider the frequency subspace $\mathbb{R}^{n \times n}$. For the low frequency domain, `DCT_Low`, we preserve components $v_{i,j}$ if $1 \leq i, j \leq n$.

For the high frequency domain, `DCT_High`, we do the opposite, masking the lowest frequency components such that n^2 components are preserved: $1 \leq i, j \leq d(1 - r_h)$. Thus $r_h d$ bands (rows/columns in V) are preserved. To ensure the number of preserved components is equal between the differently constructed masks, we specify $r_l = \frac{n}{d}$, and solve the following equation for r_h :

$$\begin{aligned} d^2 - (1 - r_h)^2 d^2 &= r_l^2 d^2 \\ 1 - (1 - r_h)^2 &= r_l^2 \\ 2r_h - r_h^2 &= r_l^2 \\ r_h^2 - 2r_h + r_l^2 &= 0 \end{aligned} \tag{3}$$

Solving the quadratic equation for $0 \leq r_h \leq 1$, $r_h = 1 - \frac{\sqrt{4(1-r_l^2)}}{2}$.

For the middle frequency band, `DCT_Mid`, we would like to ensure we mask an equal number of low and high frequency components. We thus solve the following equation for r_{ml} :

$$\begin{aligned} r_{ml}^2 d^2 &= \frac{d^2 - r_l^2 d^2}{2} \\ r_{ml} &= \sqrt{\frac{1 - r_l^2}{2}} \end{aligned} \tag{4}$$

Thus, we mask components $v_{i,j}$ if $1 \leq i, j \leq r_{ml}d$, and if $d(1 - r_{mh}) \leq i, j \leq d$. Compute r_{mh} from r_{ml} with equation 3.

For our representative random frequency mask, `DCT_Random`, much like `DCT_High`, rows/columns are chosen, except in this case randomly rather than the highest frequency bands. To ensure that n^2 components are preserved, $r_h d$ rows/columns are chosen, which are then preserved in both the x and y directions.

6.2 Complete Heatmap

We summarize our attack success rate results with Figure 6. The rows correspond to sources, and columns corresponds to targets. The sources include [Cln, Adv, Cln_1, Adv_1, Cln_3, Adv_3], where Cln is `NasNetLarge_331`, Adv is `EnsAdvInceptionResNetV2`; Cln_1, Adv_1, Cln_3, Adv_3 are summarized in the main text. The targets include [Cln, Adv, D1, D2, D3, D4], where D1~4 are defenses summarized in the main text. Thus (Cln,Cln) and (Adv,Adv) summarize white-box results, (Adv,D1~4) summarizes grey-box results, and the rest of the entries summarize black-box results. Note that the low frequency configuration is `DCT_Low` with $n = 128$.

6.3 All Plots

Figure 7 shows white-box results attacking the adversarially trained model. Figures 8-11 shows results against D1, D2, D3, and D4, respectively. Figures [12-16, 17-21, 22-26, 27-31] shows results transferring from each of the source models [Cln_1,Cln_3,Adv_1,Adv_3] to each of the target defenses [EnsAdv,D1,D2,D3,D4].

Figure 32 shows white-box results attacking the cleanly trained model. Figures 33-36 show black-box results transferring from the source models to the cleanly trained model [Cln].

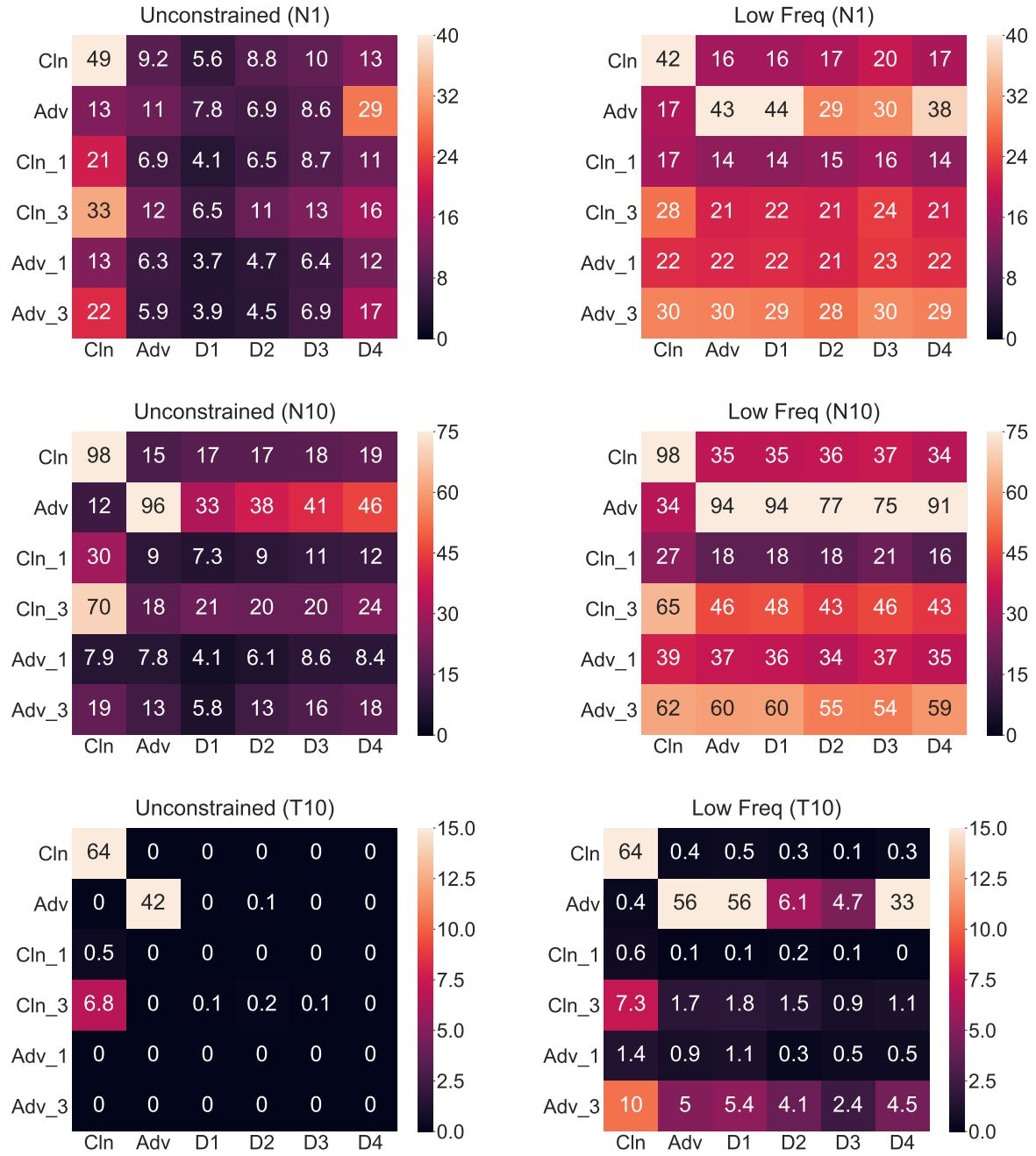


Figure 6: Transferability matrix comparing standard unconstrained MIM with low frequency constrained DCT_{Low} ($n = 128$). First, second, and third rows are non-targeted with iterations = 1, non-targeted with iterations = 10, and targeted with iterations = 10

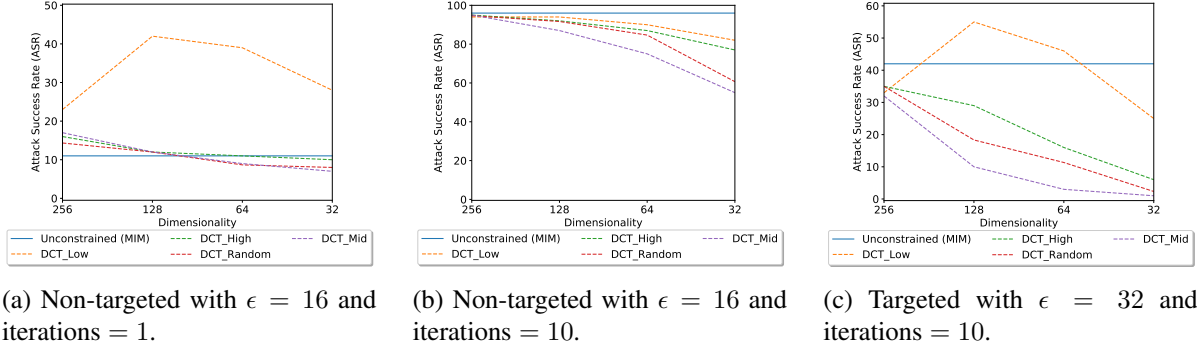


Figure 7: **White-box** attack on adversarially trained model.

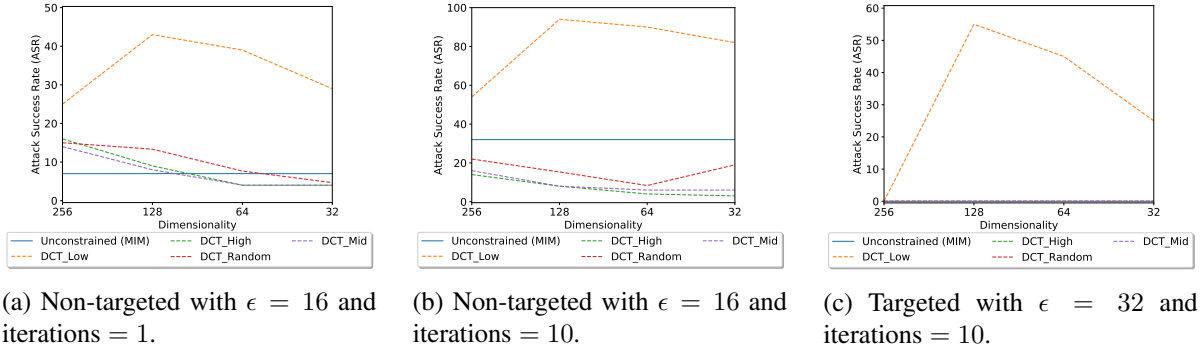


Figure 8: **Grey-box** attack on D1.

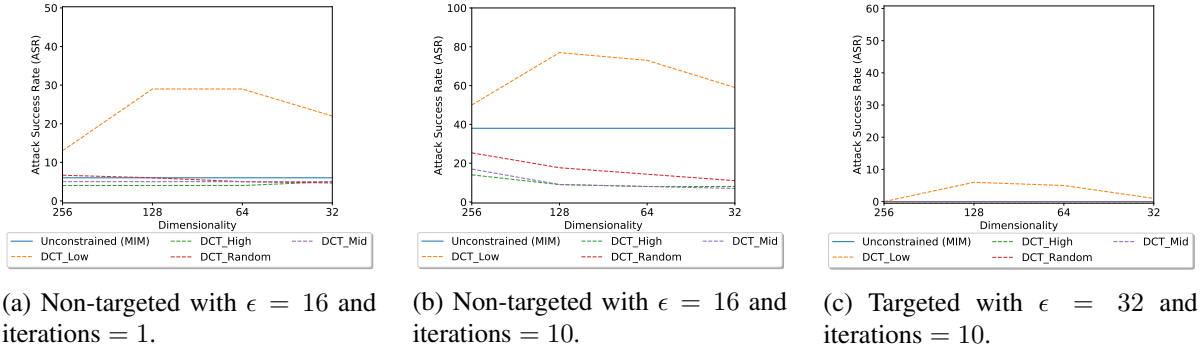


Figure 9: **Grey-box** attack on D2.

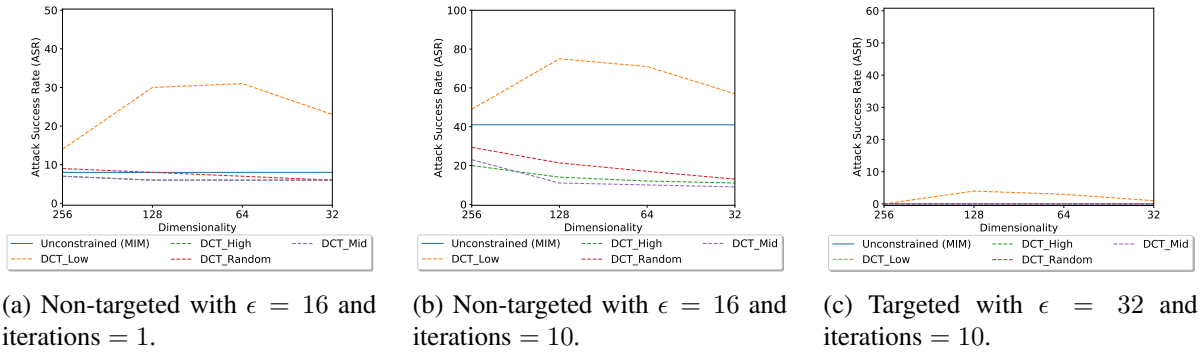
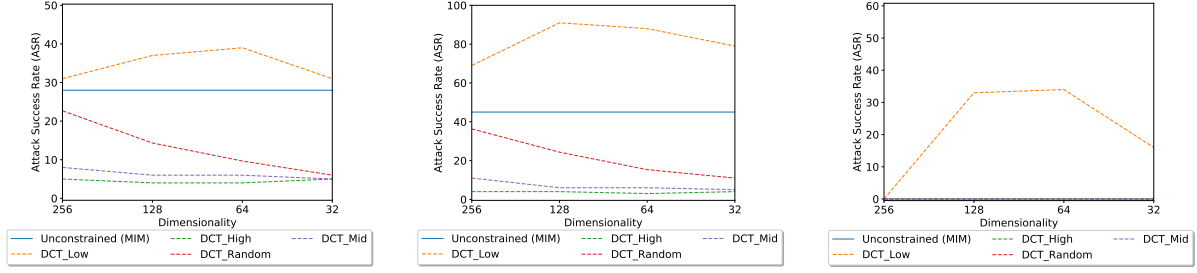


Figure 10: **Grey-box** attack on D3.

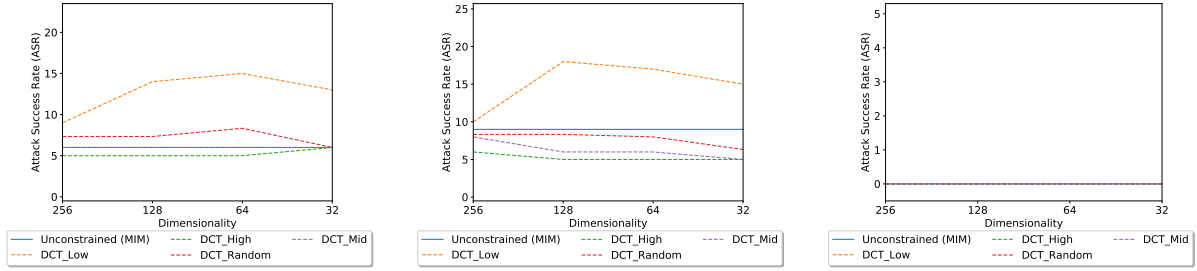


(a) Non-targeted with $\epsilon = 16$ and iterations = 1.

(b) Non-targeted with $\epsilon = 16$ and iterations = 10.

(c) Targeted with $\epsilon = 32$ and iterations = 10.

Figure 11: **Grey-box** attack on D4.

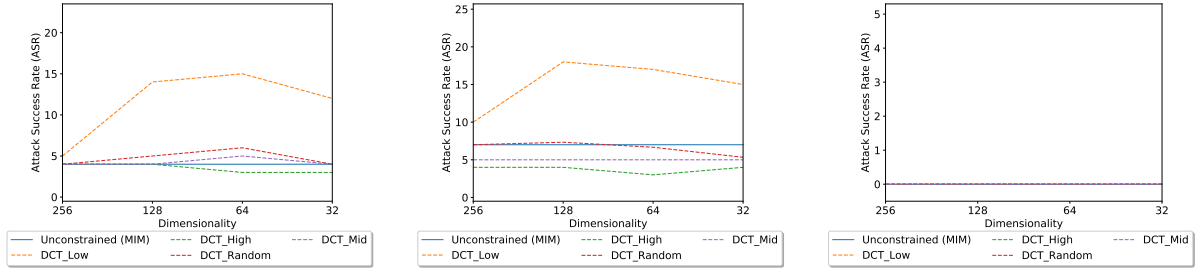


(a) Non-targeted with $\epsilon = 16$ and iterations = 1.

(b) Non-targeted with $\epsilon = 16$ and iterations = 10.

(c) Targeted with $\epsilon = 32$ and iterations = 10.

Figure 12: **Black-box** attack from Cln_1 to EnsAdv.

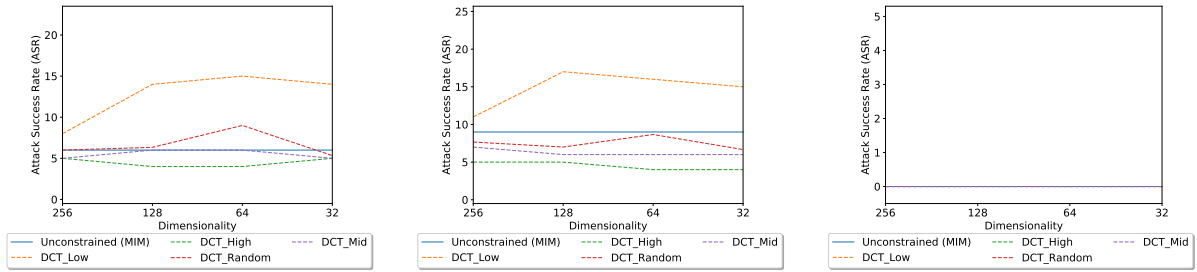


(a) Non-targeted with $\epsilon = 16$ and iterations = 1.

(b) Non-targeted with $\epsilon = 16$ and iterations = 10.

(c) Targeted with $\epsilon = 32$ and iterations = 10.

Figure 13: **Black-box** attack from Cln_1 to D1.

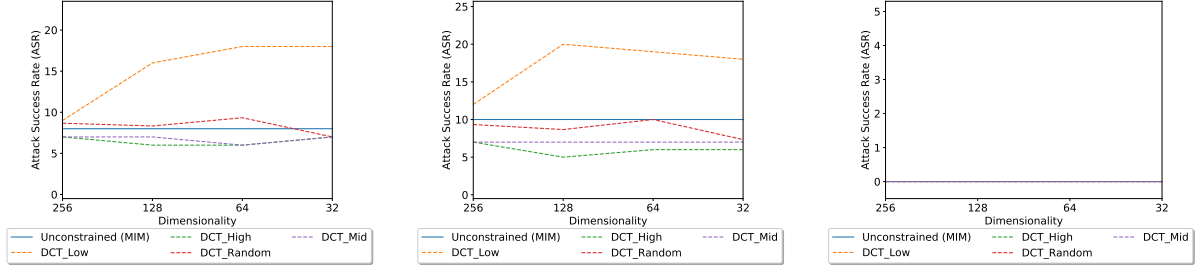


(a) Non-targeted with $\epsilon = 16$ and iterations = 1.

(b) Non-targeted with $\epsilon = 16$ and iterations = 10.

(c) Targeted with $\epsilon = 32$ and iterations = 10.

Figure 14: **Black-box** attack from Cln_1 to D2.

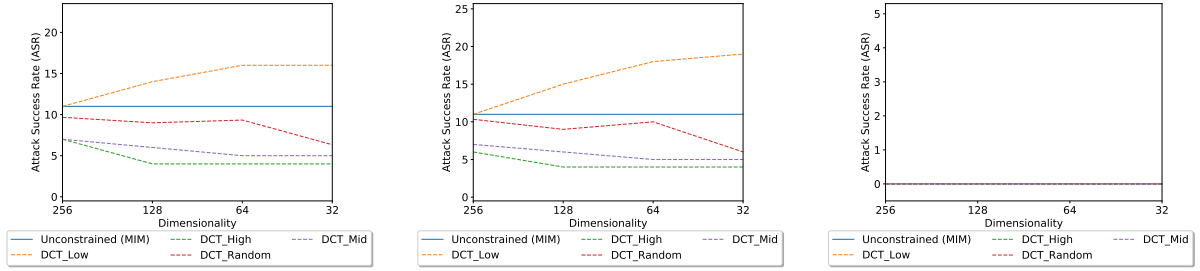


(a) Non-targeted with $\epsilon = 16$ and iterations = 1.

(b) Non-targeted with $\epsilon = 16$ and iterations = 10.

(c) Targeted with $\epsilon = 32$ and iterations = 10.

Figure 15: **Black-box** attack from Cln_1 to D3.

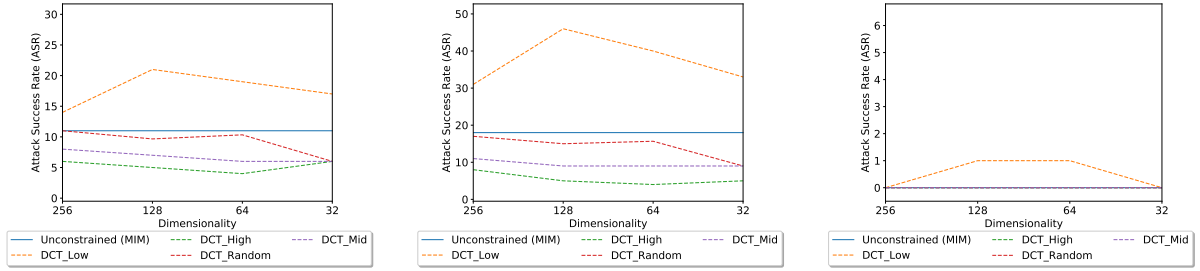


(a) Non-targeted with $\epsilon = 16$ and iterations = 1.

(b) Non-targeted with $\epsilon = 16$ and iterations = 10.

(c) Targeted with $\epsilon = 32$ and iterations = 10.

Figure 16: **Black-box** attack from Cln_1 to D4.

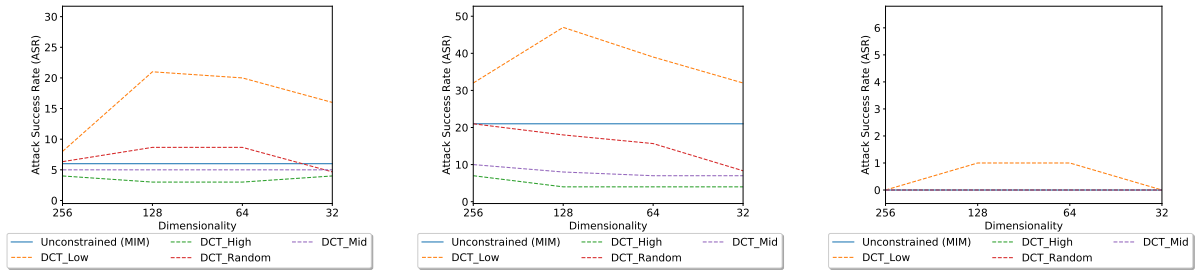


(a) Non-targeted with $\epsilon = 16$ and iterations = 1.

(b) Non-targeted with $\epsilon = 16$ and iterations = 10.

(c) Targeted with $\epsilon = 32$ and iterations = 10.

Figure 17: **Black-box** attack from Cln_3 to EnsAdv.



(a) Non-targeted with $\epsilon = 16$ and iterations = 1.

(b) Non-targeted with $\epsilon = 16$ and iterations = 10.

(c) Targeted with $\epsilon = 32$ and iterations = 10.

Figure 18: **Black-box** attack from Cln_3 to D1.

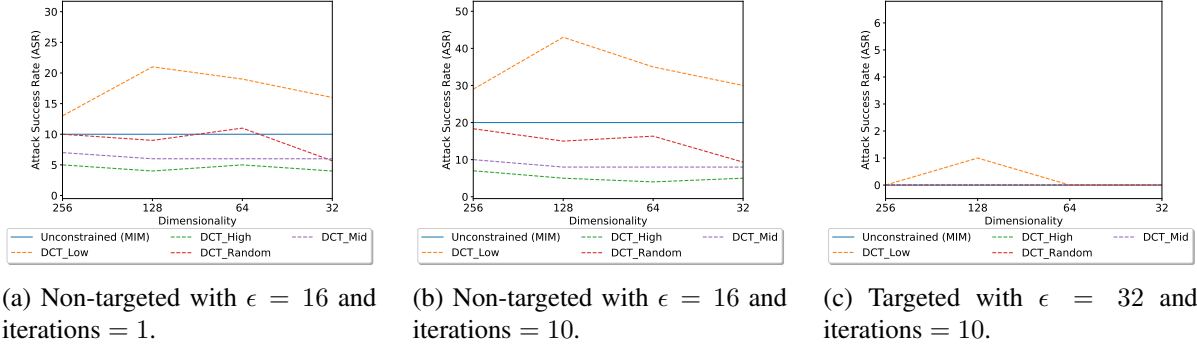


Figure 19: **Black-box** attack from Cln_3 to D2.

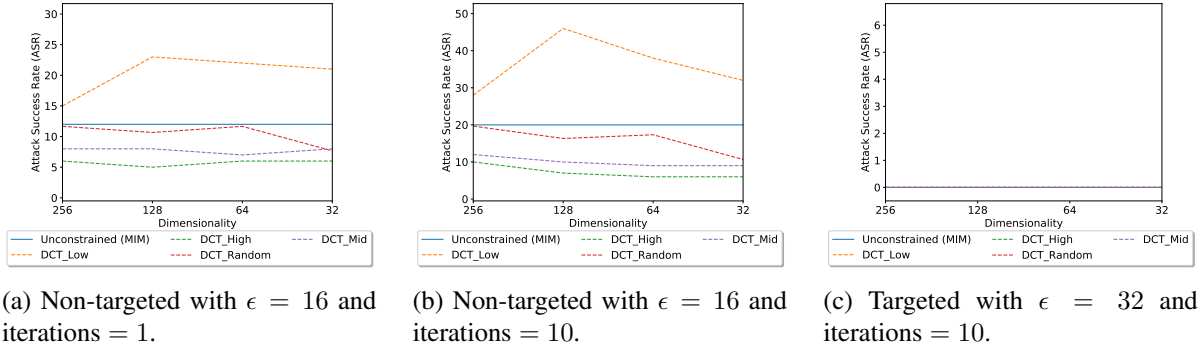


Figure 20: **Black-box** attack from Cln_3 to D3.

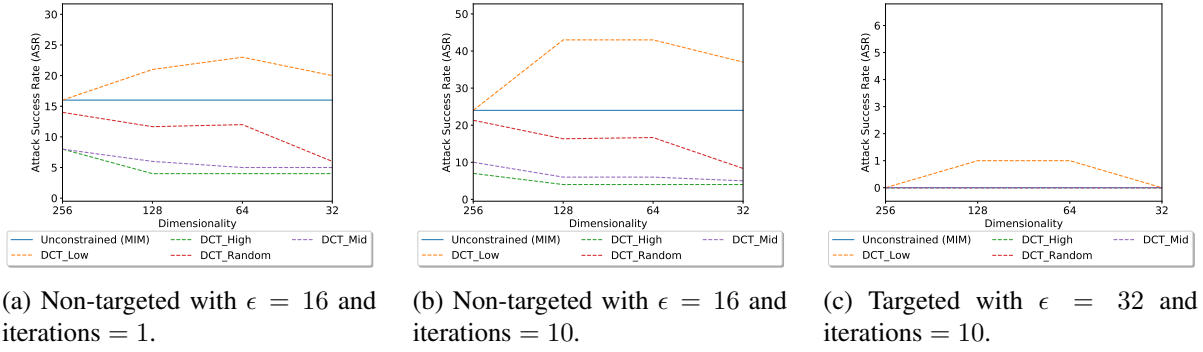


Figure 21: **Black-box** attack from Cln_3 to D4.

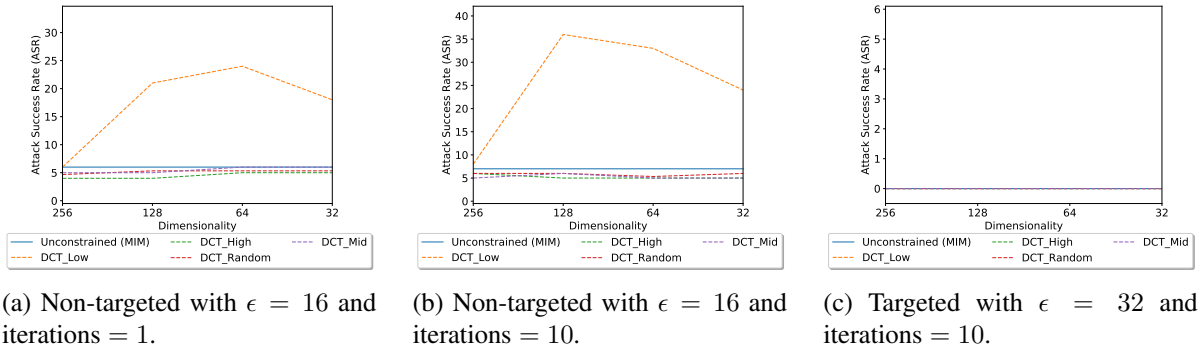
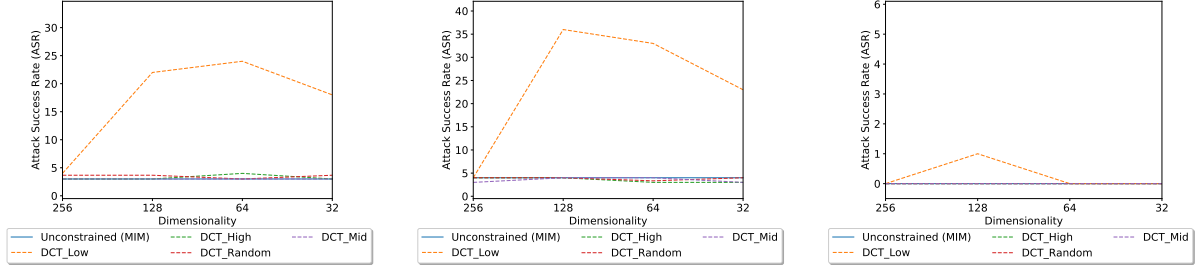


Figure 22: **Black-box** attack from Adv_1 to EnsAdv.

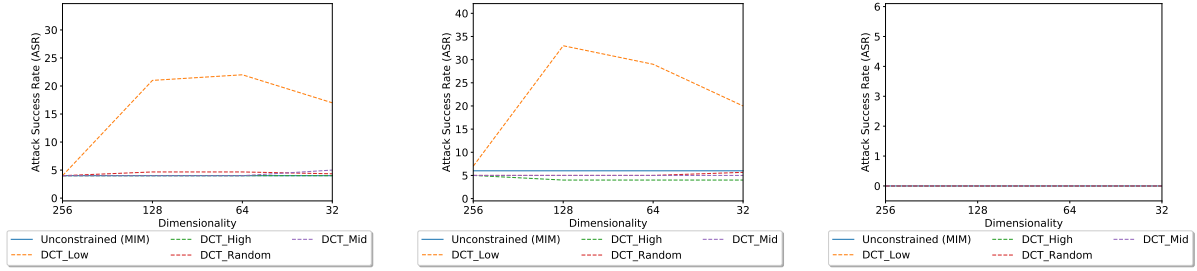


(a) Non-targeted with $\epsilon = 16$ and iterations = 1.

(b) Non-targeted with $\epsilon = 16$ and iterations = 10.

(c) Targeted with $\epsilon = 32$ and iterations = 10.

Figure 23: **Black-box** attack from Adv_1 to D1.

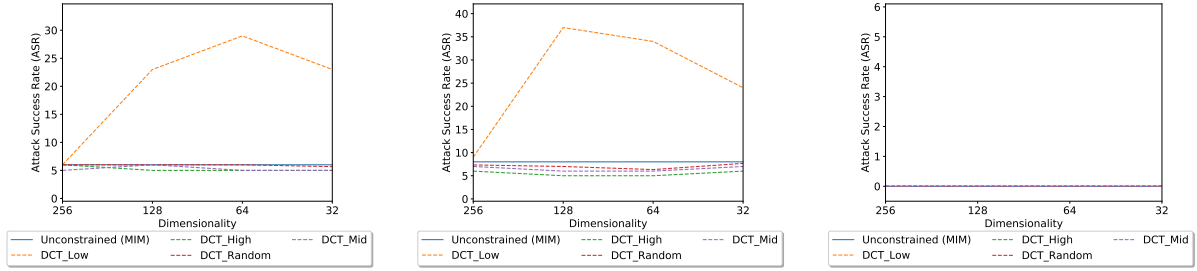


(a) Non-targeted with $\epsilon = 16$ and iterations = 1.

(b) Non-targeted with $\epsilon = 16$ and iterations = 10.

(c) Targeted with $\epsilon = 32$ and iterations = 10.

Figure 24: **Black-box** attack from Adv_1 to D2.

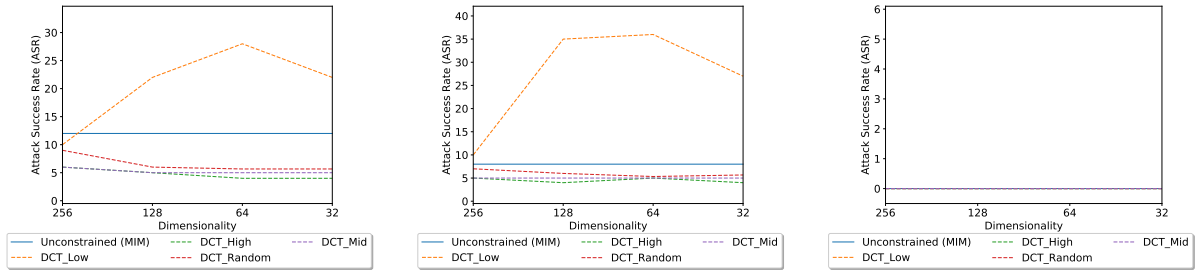


(a) Non-targeted with $\epsilon = 16$ and iterations = 1.

(b) Non-targeted with $\epsilon = 16$ and iterations = 10.

(c) Targeted with $\epsilon = 32$ and iterations = 10.

Figure 25: **Black-box** attack from Adv_1 to D3.

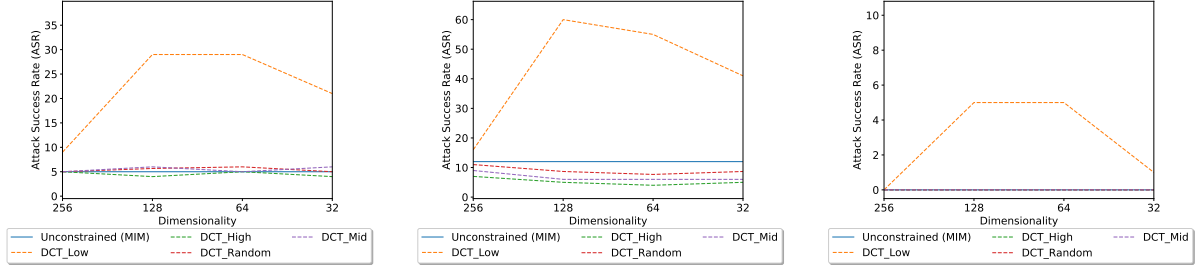


(a) Non-targeted with $\epsilon = 16$ and iterations = 1.

(b) Non-targeted with $\epsilon = 16$ and iterations = 10.

(c) Targeted with $\epsilon = 32$ and iterations = 10.

Figure 26: **Black-box** attack from Adv_1 to D4.

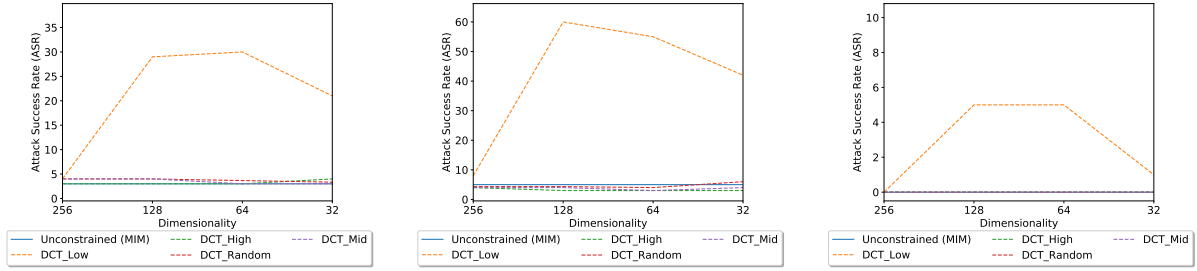


(a) Non-targeted with $\epsilon = 16$ and iterations = 1.

(b) Non-targeted with $\epsilon = 16$ and iterations = 10.

(c) Targeted with $\epsilon = 32$ and iterations = 10.

Figure 27: **Black-box** attack from Adv_3 to EnsAdv.

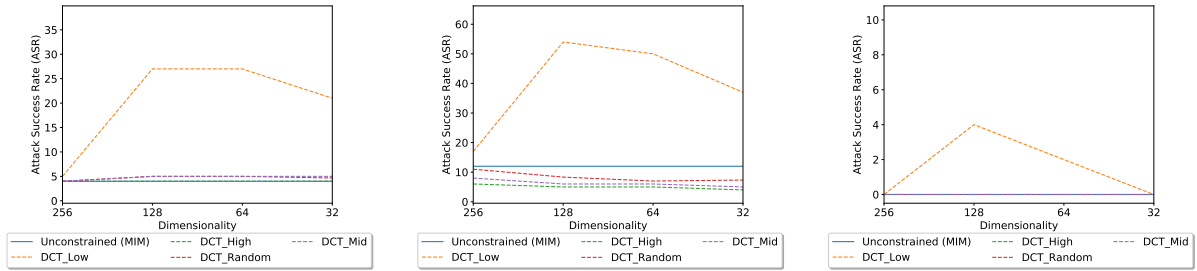


(a) Non-targeted with $\epsilon = 16$ and iterations = 1.

(b) Non-targeted with $\epsilon = 16$ and iterations = 10.

(c) Targeted with $\epsilon = 32$ and iterations = 10.

Figure 28: **Black-box** attack from Adv_3 to D1.

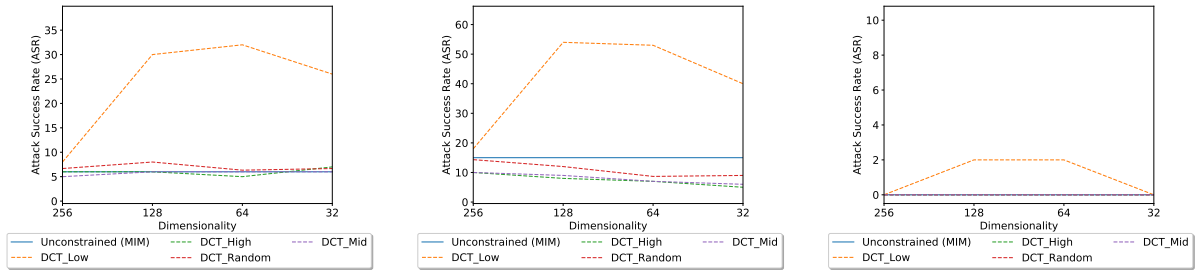


(a) Non-targeted with $\epsilon = 16$ and iterations = 1.

(b) Non-targeted with $\epsilon = 16$ and iterations = 10.

(c) Targeted with $\epsilon = 32$ and iterations = 10.

Figure 29: **Black-box** attack from Adv_3 to D2.

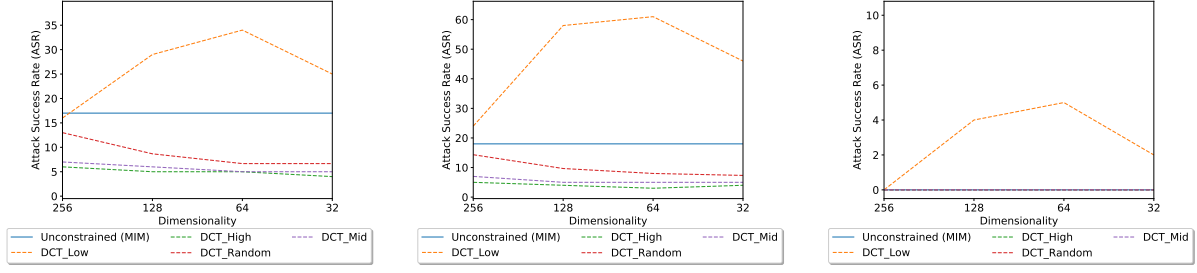


(a) Non-targeted with $\epsilon = 16$ and iterations = 1.

(b) Non-targeted with $\epsilon = 16$ and iterations = 10.

(c) Targeted with $\epsilon = 32$ and iterations = 10.

Figure 30: **Black-box** attack from Adv_3 to D3.

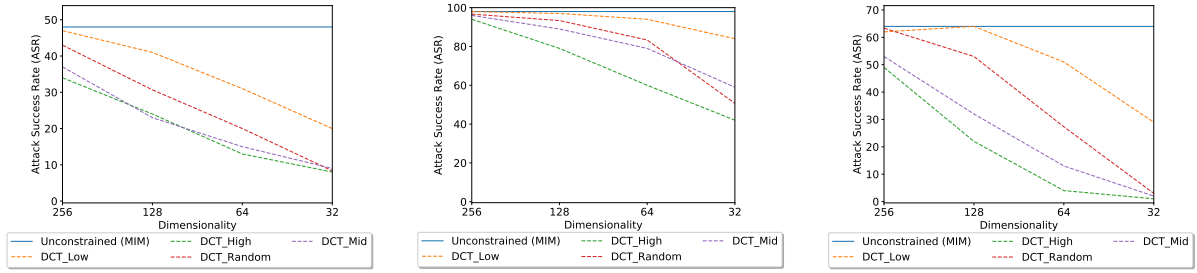


(a) Non-targeted with $\epsilon = 16$ and iterations = 1.

(b) Non-targeted with $\epsilon = 16$ and iterations = 10.

(c) Targeted with $\epsilon = 32$ and iterations = 10.

Figure 31: **Black-box** attack from Adv_3 to D4.

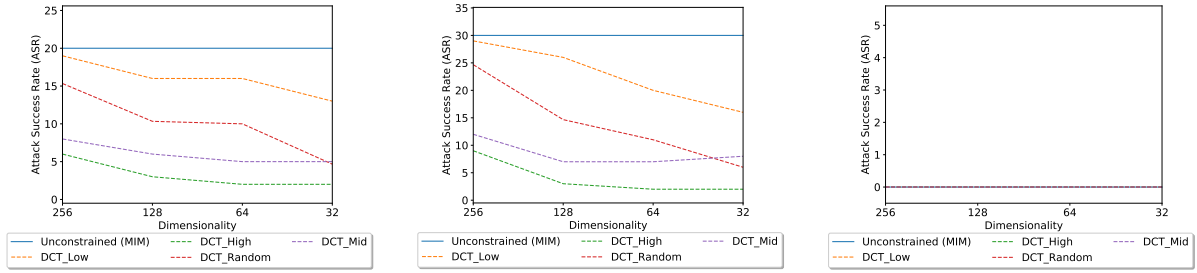


(a) Non-targeted with $\epsilon = 16$ and iterations = 1.

(b) Non-targeted with $\epsilon = 16$ and iterations = 10.

(c) Targeted with $\epsilon = 32$ and iterations = 10.

Figure 32: **White-box** attack on cleanly trained model.

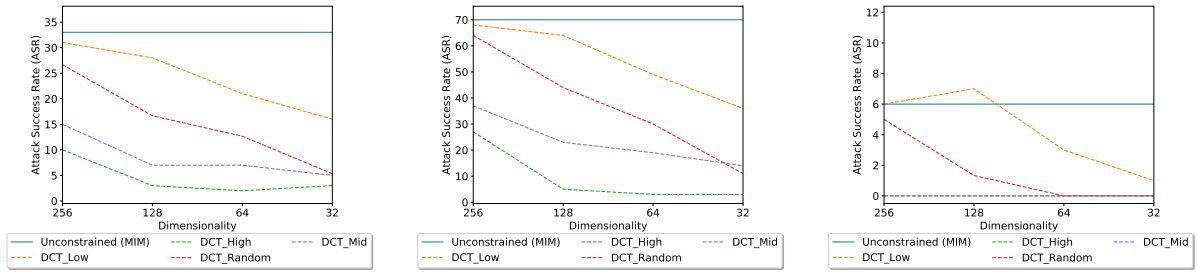


(a) Non-targeted with $\epsilon = 16$ and iterations = 1.

(b) Non-targeted with $\epsilon = 16$ and iterations = 10.

(c) Targeted with $\epsilon = 32$ and iterations = 10.

Figure 33: **Black-box** attack from Cln_1 to Cln.



(a) Non-targeted with $\epsilon = 16$ and iterations = 1.

(b) Non-targeted with $\epsilon = 16$ and iterations = 10.

(c) Targeted with $\epsilon = 32$ and iterations = 10.

Figure 34: **Black-box** attack from Cln_3 to Cln.

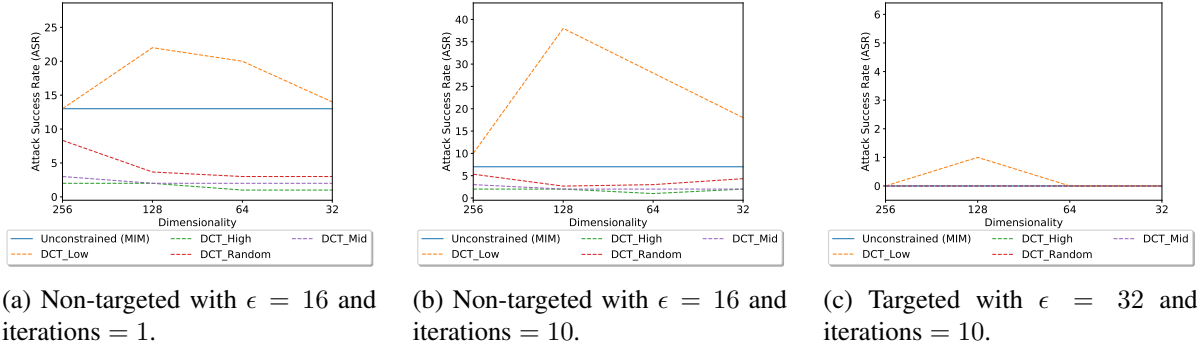


Figure 35: **Black-box** attack from Adv_1 to Cln.

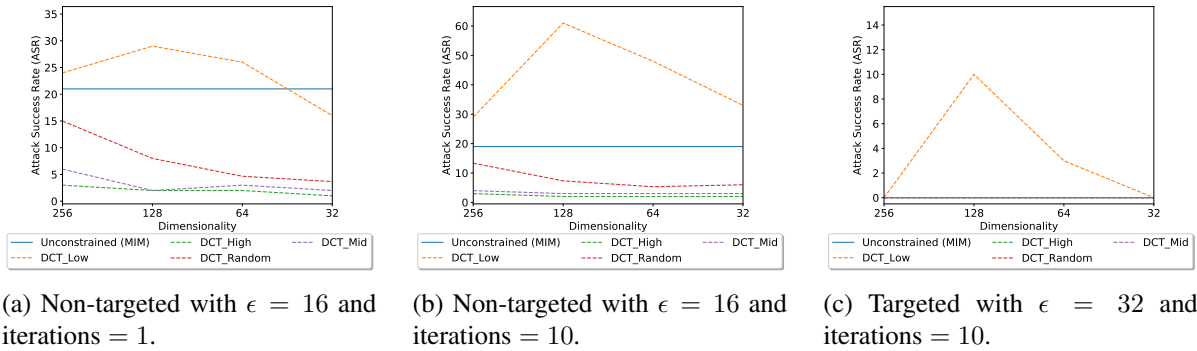


Figure 36: **Black-box** attack from Adv_3 to Cln.